Article

Electronically Activated Actin Protein Polymerization and Alignment

Ian Y. Wong, Matthew J. Footer, and Nicholas A. Melosh

J. Am. Chem. Soc., **2008**, 130 (25), 7908-7915 • DOI: 10.1021/ja7103284 • Publication Date (Web): 29 May 2008

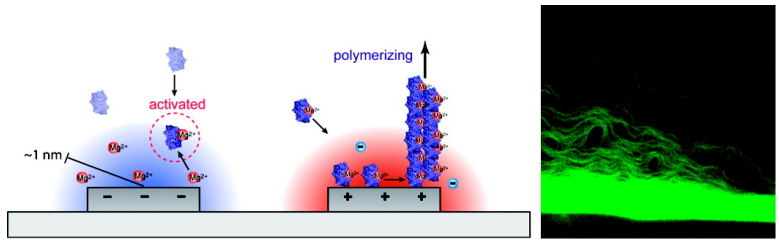

J|A|C|S
ARTICLES

Published on Web 05/29/2008

Electronically Activated Actin Protein Polymerization and Alignment

Ian Y. Wong,[†] Matthew J. Footer,[‡] and Nicholas A. Melosh*,[†]

Department of Materials Science & Engineering, Stanford University, Geballe Laboratory for Advanced Materials, 476 Lomita Mall, Stanford, California 94305, Department of Biochemistry, Stanford University School of Medicine, Beckman Center, 279 West Campus Drive, Stanford, California 94305

Received November 27, 2007; E-mail: nmelosh@stanford.edu

Abstract: Biological systems are the paragon of dynamic self-assembly, using a combination of spatially localized protein complexation, ion concentration, and protein modification to coordinate a diverse set of self-assembling components. Biomimetic materials based upon biologically inspired design principles or biological components have had some success at replicating these traits, but have difficulty capturing the dynamic aspects and diversity of biological self-assembly. Here, we demonstrate that the polymerization of ion-sensitive proteins can be dynamically regulated using electronically enhanced ion mixing and monomer concentration. Initially, the global activity of the cytoskeletal protein actin is inhibited using a low-ionic strength buffer that minimizes ion complexation and protein−protein interactions. Nucleation and growth of actin filaments are then triggered by a low-frequency AC voltage, which causes local enhancement of the actin monomer concentration and mixing with Mg^{2+}. The location and extent of polymerization are governed by the voltage and frequency, producing highly ordered structures unprecedented in bulk experiments. Polymerization rate and filament orientation could be independently controlled using a combination of low-frequency (∼100 Hz) and high frequency (1 MHz) AC voltages, creating a range of macromolecular architectures from network hydrogel microparticles to highly aligned arrays of actin filaments with ∼750 nm periodicity. Since a wide range of proteins are activated upon complexation with charged species, this approach may be generally applicable to a variety of biopolymers and proteins.

Introduction

Biological systems are dynamic entities that continuously reorganize their internal structural architectures in response to external stimuli. For instance, polymerization of actin in eukaryotic cells is highly regulated both spatially and temporally, enabling coordinated macroscopic behaviors such as cell growth, division, or motion.[1,2] This behavior has inspired the development of "smart" biomimetic materials that are responsive to external stimuli such as temperature, light, pH, and ion concentration.[3–5] In particular, there has been great interest in ion or pH-sensitive molecular components that assemble into specific morphologies such as nanofiber networks,[6,7] tubules, and membranes,[8] and hydrogels.[9–11] It is difficult however to spatially regulate component assembly in these systems at nanometer to micrometer length scales, leading to the formation of relatively homogeneous bulk materials. As a result these biomimetic systems generally lack the sophistication and functionality of higher-order directed organization in true biological systems. This also limits the use of these biomimetic systems for the deterministic fabrication of discrete artificial nanostructures.

One approach for artificially controlling biomaterial assembly is to globally inhibit activity by restricting access to activating species, such as ligands, salt, or other monomers. Assembly can then be initiated at a particular time and place through the introduction of the requisite species, such as using microfluidic delivery[12] or photochemical release.[13,14] This mechanism also occurs widely in biological systems, where transients in the concentration of small molecules, proteins, or salt trigger protein complexation and function.[15] Alternatively, locally enhancing the concentration of reactive monomers can greatly accelerate nucleation and growth rates, leading to rapid polymerization.

[†] Stanford University.
[‡] Stanford University School of Medicine.

(1) Pollard, T. D.; Borisy, G. G. *Cell* **2003**, *112*, 453–465.
(2) Rafelski, S. M.; Theriot, J. A. *Annu. Rev. Biochem.* **2004**, *73*, 209–239.
(3) Anseth, K. S.; Burdick, J. A. *MRS Bull* **2002**, *27*, 130–136.
(4) Drury, J. L.; Mooney, D. J. *Biomaterials* **2003**, *24*, 4337–4351.
(5) Mart, R. J.; Osborne, R. D.; Stevens, M. M.; Ulijn, R. V. *Soft Matter* **2006**, *2*, 822–835.
(6) Hartgerink, J. D.; Beniash, E.; Stupp, S. I. *Proc. Natl. Acad. Sci. U.S.A.* **2002**, *99*, 5133–5138.
(7) Ozbas, B.; Kretsinger, J.; Rajagopal, K.; Schneider, J. P.; Pochan, D. J. *Macromolecules* **2004**, *37*, 7331–7337.
(8) Zhang, S. G. *Nat. Biotechnol.* **2003**, *21*, 1171–1178.
(9) Fogleman, E. A.; Yount, W. C.; Xu, J.; Craig, S. L. *Angew. Chem., Int. Ed.* **2002**, *41*, 4026–4028.
(10) Petka, W. A.; Harden, J. L.; McGrath, K. P.; Wirtz, D.; Tirrell, D. A. *Science (Washington DC)* **1998**, *281*, 389–392.
(11) Topp, S.; Prasad, V.; Cianci, G. C.; Weeks, E. R.; Gallivan, J. P. *J. Am. Chem. Soc.* **2006**, *128*, 13994–13995.
(12) Burdick, J. A.; Khademhosseini, A.; Langer, R. *Langmuir* **2004**, *20*, 5153–5156.
(13) Liu, A. P.; Fletcher, D. A. *Nano Lett* **2005**, *5*, 625–628.
(14) Marriott, G. *Biochemistry* **1994**, *33*, 9092–9097.
(15) Berridge, M. J.; Lipp, P.; Bootman, M. D. *Nat. Rev. Mol. Cell. Biol.* **2000**, *1*, 11–21.

 10.1021/ja7103284 CCC: $40.75

Table 1. Selected Ion Concentrations and Debye Screening Lengths of G-Buffer, F-Buffer, Low-Salt (LS) Buffer[a]

	G-buffer (pH 8)	F-buffer (pH 7.5)	LS-buffer (pH 8)
$[Ca^{2+}]$ (mM)	2.0	0.2	
$[Mg^{2+}]$ (mM)		2.0	0.2
$[K^{+}]$ (mM)		100.0	2.0
Debye length λ_D (nm)	15.0	1.0	6.0

[a] The buffers also included 1 mM Tris, 0.2 mM ATP, and 0.1 mM DTT.

Here we investigate whether the activity of ion-sensitive proteins can be similarly regulated by exploiting the enhanced ion and monomer concentrations that exist within the diffuse-charge layer surrounding a charged electrode.

When an electrical potential difference is applied, counterions accumulate in a diffuse-charge layer at the electrode surface to screen the electric field.[16,17] For low voltages the electric potential $\psi(x)$ from the surface can be approximated by the Debye−Huckel equation, $\psi(x) = \psi_0\, e^{-x/\lambda_D}$, where λ_D is the Debye screening length. Ion concentration profiles depend upon the ion valence, z, and local potential as given by the Boltzmann distribution, $\rho(x) = \rho_\infty\, e^{-ze\psi_s/kT}$. Within the diffuse charge layer the ion concentration can be enhanced over several thousand-fold, and is particularly effective for divalent ions such as Ca^{2+} and Mg^{2+}, because their +2 valence leads to an 8-fold enhancement relative to monovalent ions. For example, a Ca^{2+} concentration wave could be artificially replicated by the application of 50 mV in a 0.1 μM $CaCl_2$ solution, leading to a 55-fold increase in Ca^{2+} at the electrode surface. Since the local ion concentration is considerably different for biomolecules situated inside and outside the layer, this approach enables electrical control localized within the nanometer scale Debye screening length. These arguments are also applicable for the local enhancement of monomer concentration. This process does not rely upon Faradic processes or redox-active molecules and thus may be applicable to a broad spectrum of proteins and synthetic molecules which are generally not electrochemically active.

One of the most dynamic biopolymers is actin, responsible for cell motility and shape.[18] Polymerized actin filaments (F-actin) are 8-nm diameter helical filaments that form by nucleation of a trimer of globular actin monomers (G-actin), and subsequently grow by the addition of G-actin to the filament termini. Polymerization of the 5 nm diameter G-actin into F-actin is highly regulated in vivo through a large number of actin-binding proteins.[1,2] In vitro, reconstituted G-actin can be maintained in its monomeric state by a low ionic strength medium and millimolar Ca^{2+} levels (Table 1).[19] Inactivity in this "G-buffer" is thought to be caused by Ca^{2+} binding in the high-affinity binding site of G-actin, which changes the structural conformation[20] and significantly increases the critical concentration of monomer necessary for polymerization relative to Mg^{2+}-bound G-actin.[21] Polymerization of G-actin into F-actin can be initiated by increasing the ionic strength to physiological levels and adding millimolar concentrations of Mg^{2+}, which promotes the replacement of Ca^{2+} by Mg^{2+} in the high-affinity site.[22–27] Since F-actin polymerization is an important, dynamic biochemical process that exhibits sensitivity to divalent ion concentration but no redox activity, it is an ideal model system with which to investigate electrostatically activated self-assembly.

Actin polymerization falls into a broad class of protein assembly which requires initial activation of the monomer (Mg^{2+} here), followed by nucleation and growth (−11e charged G-actin). Since the activating and monomer species have opposite charges and are freely diffusing in solution, it is not intuitive how these two species can be concentrated at the same location using electrostatics. The experiments below demonstrate that this class of polymerization reaction can indeed be electrostatically actuated by a low-frequency AC bias, which encourages both mixing and growth. Frequency-dependent measurements indicate the polymerization rate is controlled by a competition between mixing and nucleation, while the filament morphology is largely determined by electrokinetic effects. Polymerization was observed from 10−500 Hz, while higher frequencies (1 kHz to 1 MHz) did not induce polymerization but could dielectrophoretically align long actin filaments.[28] These separate regimes provide independent control of growth and orientation which can be exploited for formation of ordered nanostructures. These results demonstrate that the unique electrostatic conditions at the electrode surface can modulate self-assembly of free species in solution even without electrochemical reactivity and provide excellent spatial and temporal control.

Experimental Design

In these experiments G-actin was suspended in a low-salt (LS) buffer containing a small amount of Mg^{2+} formulated to inhibit global actin polymerization (Table 1), yet provide the necessary ionic conditions when concentrated in an electric field. The low-salt buffer had 0.20 mM Mg^{2+} and a Debye screening length of 6.0 nm, intermediate between F-buffer and G-buffer. The LS buffer successfully inhibited F-actin polymerization, as control samples of 5.0 μM G-actin in LS-buffer (including fluorescent phalloidin dye) showed no polymerization after 2 h. In addition, a sedimentation assay[29] under these conditions also showed no polymerization after 24 h, consistent with previous measurements of G-actin critical concentration at low concentrations of Mg^{2+}.[30]

Electrostatically induced polymerization was investigated by placing 5 μM Ca^{2+}-complexed G-actin in LS-buffer on top of a glass wafer with opposing titanium electrodes with electrode gaps that varied from 1−300 μm (Figure 1a). Titanium was chosen for its robust native oxide layer, which inhibits direct electron transfer. Electrolysis of water was observed at voltages of 3.5 V, so applied potentials were maintained at ±2.5 V in all experiments. However, the TiO_2 dielectric layer causes a considerable reduction in the

(16) Bard, A. J.; Faulkner, L. R. *Electrochemical Methods: Fundamentals and Applications*, 2nd ed.; Wiley: Hoboken, NJ, 2001.
(17) Hunter, R. J., *Foundations of Colloid Science*, 2nd ed.; Clarendon Press, New York, 2001.
(18) Straub, F. B. *Stud. Inst. Med. Chem. Univ. Szeged* **1942**, *2*, 1–15.
(19) Spudich, J. A.; Watt, S. *J. Biol. Chem.* **1971**, *246*, 4866–71.
(20) Guan, J. Q.; Almo, S. C.; Reisler, E.; Chance, M. R. *Biochemistry* **2003**, *42*, 11992–12000.
(21) Kinosian, H. J.; Selden, L. A.; Estes, J. E.; Gershman, L. C. *Biochim. Biophys. Acta* **1991**, *1077*, 151–158.
(22) Carlier, M.-F.; Pantaloni, D.; Korn, E. D. *J. Biol. Chem.* **1986**, *261*, 10778–10792.
(23) Cooper, J. A.; Buhle, E. L.; Walker, S. B.; Tsong, T. Y.; Pollard, T. D. *Biochemistry* **1983**, *22*, 2193–2202.
(24) Frieden, C. *Proc. Natl. Acad. Sci. USA* **1983**, *80*, 6513–6517.
(25) Gershman, L. C.; Newman, J.; Selden, L. A.; Estes, J. E. *Biochemistry* **1984**, *23*, 2199–2203.
(26) Pollard, T. D. *Anal. Biochem.* **1983**, *134*, 406–412.
(27) Tobacman, L. S.; Korn, E. D. *J. Biol. Chem.* **1983**, *258*, 3207–3214.
(28) Asokan, S. B.; Jawerth, L.; Carroll, R. L.; Cheney, R. E.; Washburn, S.; Superfine, R. *Nano Lett.* **2003**, *3*, 431–437.
(29) Sanders, M. C.; Way, M.; Sakai, J.; Matsudaira, P. *J. Biol. Chem.* **1996**, *271*, 2651–2657.
(30) Tobacman, L. S.; Brenner, S. L.; Korn, E. D. *J. Biol. Chem.* **1983**, *258*, 8806–8812.

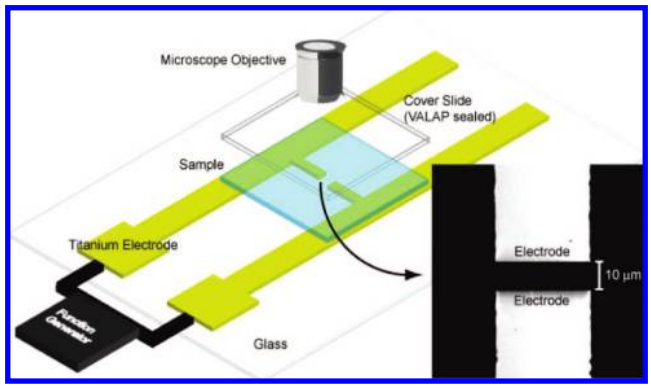

Figure 1. Microfabricated electrodes in a fluidic sample chamber can be used for voltage-induced F-actin polymerization. The 50-nm thick titanium electrodes are fabricated on a glass substrate and contacted to an arbitrary function voltage generator. The fluid sample is sandwiched between electrodes and a cover slide and sealed to form a sample chamber approximately 10-μm thick. Polymerization is characterized using optical fluorescence microscopy. (Inset) Scanning electron micrograph shows a 10-μm gap between titanium electrode pairs.

electrostatic potential at the electrode surface compared to the applied voltage. The potential at the TiO_2−water interface was found by iteratively varying the charge density on the metal and calculating the resulting net potential drop across the dielectric and solution phase. The full Poisson−Boltzmann equation was used to calculate these ion-distributions rather than the linearized Debye−Hückel approximation, which is only valid for potentials much smaller than $kT/e \approx 25$ mV.[16,17] This process is repeated until a net voltage drop $V_{applied}/2$ is obtained for each electrode. For an applied voltage of 2.5 V in LS-buffer, the calculated surface potential is ~100 mV. At this surface potential, the G-actin concentration calculated using a modified Poisson−Boltzmann equation[31] was two densely packed monolayers ~ 9 nm thick, rapidly dropping to bulk concentration at 13 nm.[32] Magnesium ions in LS buffer were calculated to have a surface concentration of 600 mM, dropping to 50 mM at 2 nm and 1 mM at 9 nm.

For AC voltages, a square-wave potential of ±2.5 V is used to mitigate electro-osmotic flow, which can be significant with sinusoidal waveforms. The pulse risetime is limited by ion accumulation at the electrode surfaces, but less than 0.1 ms in all cases. Due to the short risetime, the potential field and consequent ion calculations at the electrode surface are assumed to be effectively at DC and solved using the full PB equation. During the transition period the ion concentrations vary considerably, and currently no attempt is made to model the temporal concentration distributions.

Actin polymerization was visualized through the addition of fluorescent Alexa 488 phalloidin, which binds selectively to F-actin. Although phalloidin allows filament visualization, it also decreases the critical concentration of G-actin by 10−30 fold[33] and essentially eliminates depolymerization. However, phalloidin alone was insufficient to induce polymerization, as no filaments were observed in control experiments containing phalloidin up to 24 h.

Results and Discussion

Activation and polymerization of G-actin in LS buffer was studied under DC and AC bias conditions to investigate mixing and nucleation effects. Initially, a DC bias up to ±2.5 V was applied. No actin polymerization was ever observed under any DC bias conditions. This result is somewhat surprising as Ca^{2+} bound G-actin had been observed to form monolayers of F-actin strands at the surface of highly charged cationic lipid bilayers.[34–36] However, due to the opposite charges of Mg^{2+} and G-actin ($-11e$) they concentrate at opposing electrodes and do not mix appreciably. If actin polymerization could be initiated solely by favoring nucleation and growth within the highly concentrated layer of Ca^{2+}-bound actin at the electrode surface, polymerization should have been observed at DC bias. This was not the case, leading us to conclude that mixing with Mg^{2+} was essential for polymerization to occur. This limitation could conceivably be circumvented if the reactive species were immobilized at the electrode surface, restraining them even under unfavorable bias.

AC-Modulated Actin Polymerization. The application of low-frequency AC electric fields from 10−1000 Hz successfully initiated local polymerization of actin at the electrode surfaces in LS-buffer. A representative example of polymerization is shown in Figure 2 for a 100 Hz, ±2.5 V square-wave voltage with a 10 μm electrode separation. After applied voltage was initiated there was a uniform increase in fluorescence throughout the frame at 30 s, indicating the formation of stable actin nuclei that were freely diffusing. Distinct fibrillar structures became visible between 30−60 s, forming parallel to the electrode surface and subsequently increasing in thickness and intensity. Lower magnification images confirmed that filament growth only occurred at the electrode edges and nowhere else in the sample (Figure 2, right). Over a period of 10 min at 100 Hz, the polymerized actin filaments at the electrode edges grew inward until they merged into one. As polymerization progressed, the accumulated F-actin assumed a convex shape as the outermost filaments began to lose their parallel alignment. Continuation of this process led to merging of the actin filaments from separate electrodes, after which the fluorescence intensity continued to increase at ~3% per minute while the size of the mass remained approximately the same, indicating the density of polymerized F-actin was increasing. The amount of actin polymerized on each electrode was approximately equal, although asymmetric growths did occasionally occur.

The rapid formation of small actin filaments or nuclei throughout the entire image indicates that nucleation occurs at all electrode surfaces. These small species cannot be resolved optically and after formation diffuse throughout the image area, resulting in the nearly uniform increase in fluorescence immediately after voltage is applied. In contrast, larger filaments that can be resolved are only observed at the electrode edges. We believe this localization is due to dielectrophoretic trapping of small actin nuclei or filaments, which only occurs at the highest electric field gradients for these 10−15 nm particles. Once trapped, these filaments continue to grow which further restricts them to the surface and generates the observed bundle-like structures. Away from the electrode edges, the electric field gradient is too low to trap any of the nuclei, which rapidly diffuse away into the surrounding area.

To verify the biochemical functionality of the electronically activated actin and visualize the morphology more clearly, 5 μM of α-actinin, a complementary binding protein, was added to the sample solution. This well-known bundling protein is a rodlike molecule approximately 30 nm long, which forms an

(31) Borukhov, I.; Andelman, D.; Orland, H. *Phys. Rev. Lett.* **1997**, *79*, 435.
(32) Wong, I. Y.; Footer, M. J.; Melosh, N. A. *Soft Matter* **2007**, *3*, 267–274.
(33) Cooper, J. A. *J. Cell. Biol.* **1987**, *105*, 1473–1478.
(34) Renault, A.; Lenne, P. F.; Zakri, C.; Aradian, A.; Venien-Bryan, C.; Amblard, F. *Biophys. J.* **1999**, *76*, 1580–1590.
(35) Wong, G. C. L.; Tang, J. X.; Lin, A.; Li, Y. L.; Janmey, P. A.; Safinya, C. R. *Science* **2000**, *288*, 2035–2039.
(36) Laliberte, A.; Gicquaud, C. *J. Cell. Biol* **1988**, *106*, 1221–1227.

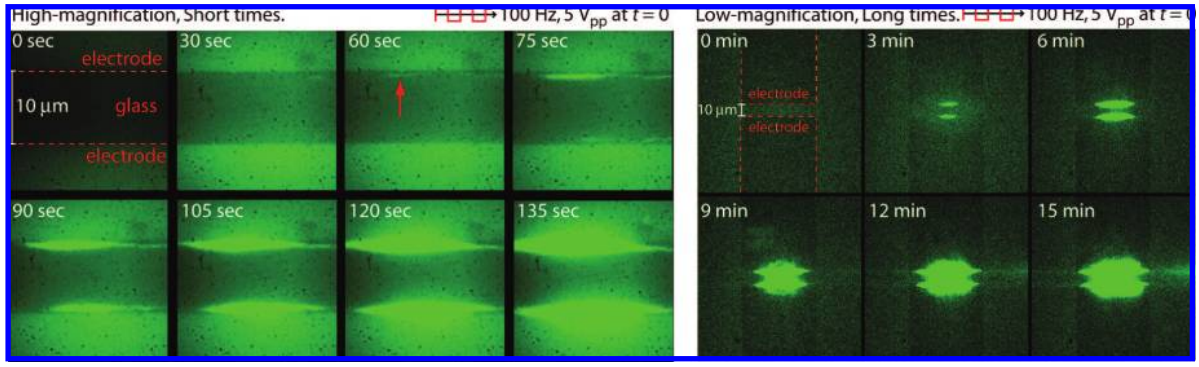

Figure 2. (left) F-Actin polymerizes at the edges of two electrodes spaced 10 μm apart during a 100 Hz, 5 V_{pp} square-wave bias. Actin filaments parallel to the electrodes are first observed at 60 s, subsequently increasing in intensity and width. (right) As F-actin continues to polymerize due to Mg^{2+}-binding in the applied field, the filaments grow from either electrode, eventually merging into one mass as polymerization progresses. Filaments are most concentrated at the electrode edge.

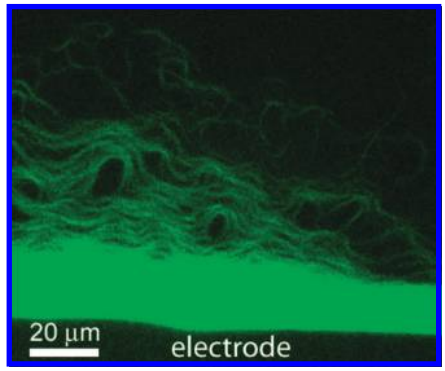

Figure 3. Visible actin bundles stacked with nematic ordering after 180 min with the addition of 5 μM α-actinin. The electrode gap was 300 μm to enable clear visualization of the filaments.

antiparallel homodimer with actin-binding regions on each end.[37,38] Figure 3 shows discrete bundles characteristic of α-actinin/actin that formed parallel to the electrode surface. These bundles were hundreds of micrometers long and concentrated parallel to the electrode edges. These structures have two levels of hierarchical order: actin filaments bundled together by α-actinin and the bundles packed into a nematic configuration. The highly ordered actin configuration is unlike bulk experiments, where α-actinin/actin form random isotropic gels.[38] Some actin alignment has been previously observed at elevated concentrations of divalent ions (~10 mM Mg^{2+}) leading to salt-bridging bundles with diameters limited to ~300 nm,[39–42] or by actin polymerization within microfluidic channels[43] with lower density.

The nematic ordering of these structures is consistent with actin filaments polymerizing along the electrode surface, then becoming displaced as new filaments begin to form. This mechanism is distinct from bulk experiments, where the uniform distribution of activated monomers allows filaments to grow at

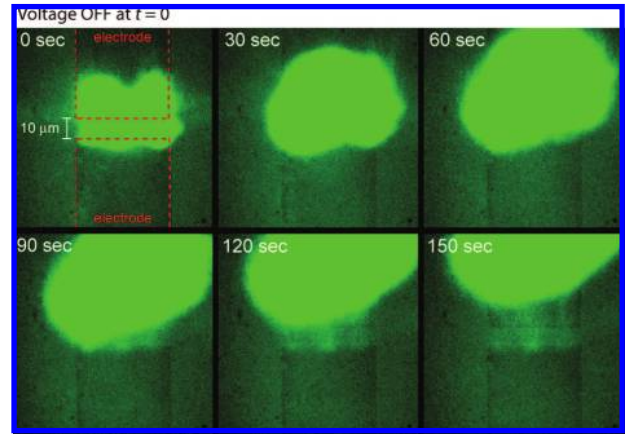

Figure 4. Physically cross-linked hydrogel microparticles ("microgels") of polymerized F-actin remain intact if the actin filaments from either electrode coalesce, even after AC voltage is switched off. Successive images at 30 s intervals show an expansion in size before the mass drifts out of the field of view.

any location and in any direction.[26] We see no evidence that filaments continue to grow once displaced from the electrode surface and the filament density is always highest at the electrode edge. The high degree of nematic order is also apparently metastable as filaments begin to lose their alignment farther from the electrode surface. Similarly, if the electrode potential is turned off the filaments slowly reorient and exfoliate from the surface. Exfoliation is slow (~minutes), suggesting the filaments even far from the electrode have limited mobility which may arise from steric entanglements or salt bridges. Intriguingly, a recent study found nematic-phase actin filaments had decreased longitudinal diffusion at high divalent counterion concentrations,[44] attributed to attractive salt-bridging effects. The high concentration of Mg^{2+} at the electrode surface in our system may induce local salt-bridging, which gradually dissociates as the filaments are displaced from the surface.

F-actin Entanglement. Actin gels can be formed if actin polymerization is allowed to bridge the gap between electrodes, resulting in a mass of actin that remains intact even with the removal of the AC voltage (Figure 4). After the voltage is turned off, these actin microgels typically swell in size by a factor of 2, and diffuse away as a single object. This demonstrates that the actin filaments are not attached to the electrodes, and that

(37) Meyer, R. K.; Aebi, U. *J. Cell. Biol* **1990**, *110*, 2013–2024.
(38) Wachsstock, D. H.; Schwarz, W. H.; Pollard, T. D. *Biophys. J.* **1993**, *65*, 205–214.
(39) Tang, J. X.; Janmey, P. A. *J. Biol. Chem.* **1996**, *271*, 8556–8563.
(40) Kwon, H. J.; Kakugo, A.; Shikinaka, K.; Osada, Y.; Gong, J. P. *Biomacromolecules* **2005**, *6*, 3005–3009.
(41) Wong, G. C. L.; Lin, A.; Tang, J. X.; Li, Y.; Janmey, P. A.; Safinya, C. R. *Phys. Rev. Lett.* **2003**, *91*, 018103.
(42) Lai, G. H.; Coridan, R.; Zribi, O. V.; Golestanian, R.; Wong, G. C. L. *Phys. Rev. Lett.* **2007**, *98*, 187802.
(43) Hirst, L. S.; Parker, E. R.; Abu-Samah, Z.; Li, Y.; Pynn, R.; MacDonald, N. C.; Safinya, C. R. *Langmuir* **2005**, *21*, 3910–3914.
(44) He, J.; Viamontes, J.; Tang, J. X. *Phys. Rev. Lett.* **2007**, *99*, 068103.

the actin filaments experience appreciable dielectrophoretic force even at low applied frequencies. Such freestanding gel microstructures have not been previously demonstrated using cytoskeletal proteins, but similar physically cross-linked hydrogel microparticles ("microgels") have technological applications as microreactors, biosensors, and drug delivery platforms.[45]

Gel-formation likely occurs as reoriented actin filaments at the interface region undergo a crossover from a dilute semiflexible polymer phase to an entangled gel phase, as the purely nematic structures were never stable. This critical filament number density can be estimated by $c^{**} \approx L^{-3}\sqrt{(L_p/L)}$ in the rodlike limit for filament contour lengths L much smaller than the persistence length L_p.[46] For a persistence length $L_p = 17$ μm for phalloidin-bound actin[47] and a typical experimental contour length $L \approx 2$ μm, the transition filament number density is $c^{**} = 3.6 \times 10^{17}$ m^{-3}, which is equivalent to a bulk polymer gel formed at a concentration of 0.44 μM G-actin. This calculation is a lower bound as some filament anisotropy is likely retained. An upper bound on the filament concentration is provided by the isotropic to nematic transition, which would cause all the filaments to remain aligned. This transition can be estimated in the short-rod limit as $c_{nem} = 4.3/(dL^2)$.[46] Using the F-actin diameter $d = 8$ nm, $c_{nem} = 1.5 \times 10^{20}$ m^{-3} which would correspond to a bulk polymer gel formed from 188 μM G-actin. The actual filament density in the entangled region is thus likely between $10^{17}-10^{20}$ m^{-3}, intermediate to the limiting cases of an isotropic entangled network (c^{**}) and a fully anisotropic nematic phase (c_{nem}).

Actin Polymerization Kinetics and Mechanism. Insight into the mechanisms that govern voltage-induced polymerization can be gained by comparing the frequency-dependent polymerization kinetics (Figure 5A) to bulk polymerization assays (Figure 5A, inset). In bulk solution polymerization proceeds through an initial activation step where Ca^{2+} is exchanged for Mg^{2+} in the tight binding site of G-actin.[23,24] Subsequently, there is a lag-time associated with the kinetically slow reaction of three G-actin monomers to form stable trimeric F-actin nuclei,[23,24,27] followed by a growth period where existing F-actin filaments elongate. At long times, the polymerization curve approaches a plateau as the bulk concentration of actin monomers is depleted and the reaction approaches steady-state.[48,49]

The fluorescence intensity of F-actin polymerization for $\nu =$ 0, 10, 100, 200, and 1000 Hz are shown in Figure 5A. The polymerization curves all begin with an initial lag-time followed by a constant linear slope of increasing fluorescence, analogous to the nucleation and elongation regimes observed in bulk. Unlike bulk polymerization, the AC voltage-induced polymerization curves do not approach a steady-state plateau, indicating that polymerization at the electrodes does not significantly deplete the bulk monomer concentration. The lag-times increased with frequency, from 30 s at 10 Hz to infinity at 1000 Hz and above (Figure 5B, plotted as inverse lag-time vs frequency) indicating nuclei formation becomes slower with increasing frequency. In the elongation regime polymerization

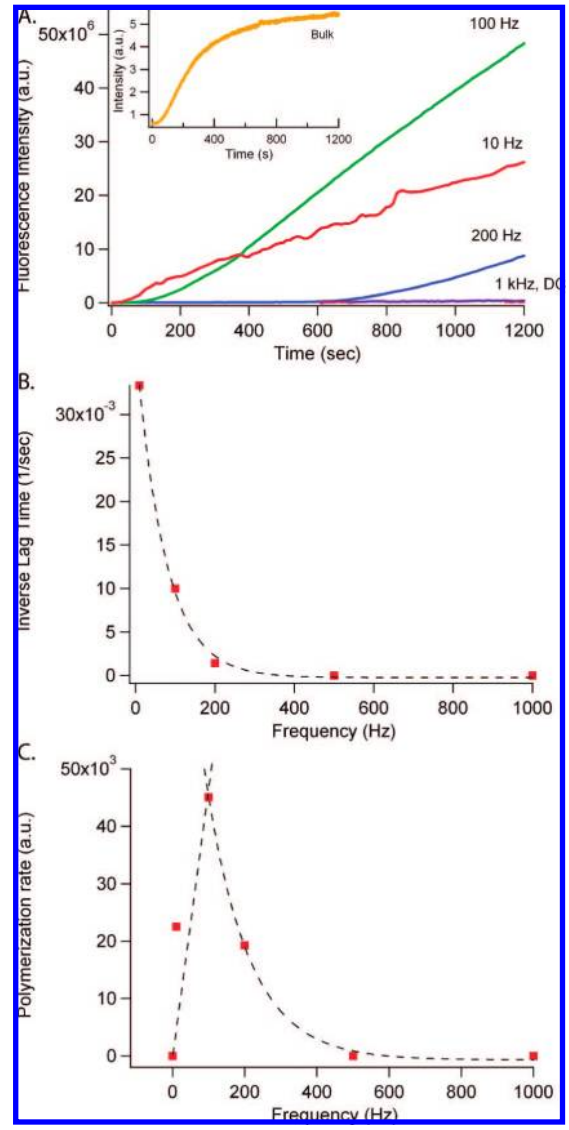

Figure 5. (A) Kinetics of AC voltage-induced F-actin polymerization measured from changes in fluorescence intensity. For frequencies where polymerization occurs, the kinetics are characterized by a lag period and a constant linear slope. AC square wave voltages are a constant 2.5 V: pink, DC; red, 10 Hz; green, 100 Hz; blue, 200 Hz; purple, 1000 Hz. (Inset) Bulk F-actin polymerization under physiological salt conditions.[50] (B) The inverse lag time decreases as a function of frequency. (C) F-actin polymerization rates from part (A).

rate increased approximately linearly from 0 (DC)−100 Hz, then decreased exponentially to zero at 1 kHz (Figure 5C). Based on kinetic models of bulk polymerization, the polymerization rate depends upon the availability of Mg^{2+}-complexed G-actin monomers as well as the number of reactive actin filament termini. The linearity of this regime suggests that polymerization is rate-limited at a single site (the electrode surface) rather than at filament ends located in the bulk solution which would accelerate growth as more actin nuclei were produced. This is consistent with the highest actin filament density at the interface and no growth away from the electrodes.

The observed lag-time and polymerization kinetics suggest competition between mixing and nucleation processes with opposite frequency dependence control actin activation and polymerization. The fact that no polymerization occurs under DC bias indicates very high actin concentrations alone at the electrode surface are not sufficient to induce polymerization,

(45) Das, M.; Zhang, H.; Kumacheva, E. *Annu. Rev. Mater. Res.* **2006**, *36*, 117–142.
(46) Morse, D. C. *Macromolecules* **1998**, *31*, 7030–7043.
(47) Ott, A.; Magnasco, M.; Simon, A.; Libchaber, A. *Phys. Rev. E* **1993**, *48*, R1642–R1645.
(48) Carlier, M. F. *J. Biol. Chem.* **1991**, *266*, 1–4.
(49) Pollard, T. D.; Cooper, J. A. *Annu. Rev. Biochem.* **1986**, *55*, 987–1035.
(50) Mullins, R. D.; Machesky, L. M. *Methods Enzymol.* **2000**, *325*, 214–237.

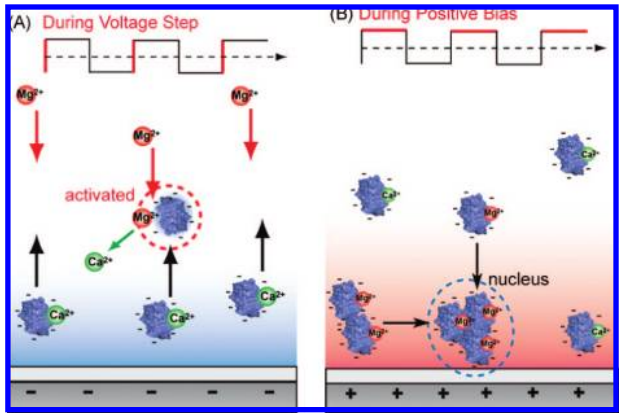

Figure 6. (A) Nonequilibrium mixing between oppositely charged Mg^{2+} and actin species occurs during the transition between opposite bias polarities. Increasing frequency increases the amount of mixing, up to the ability of the reagents to respond to the field. (B) During positive potential Mg^{2+}-actin is concentrated at the electrode surface, increasing nuclei formation and growth rates. Nuclei formation requires accumulation of actin, which decreases as the frequency approaches the mobility limit for actin.

but mixing with Mg^{2+} is necessary. Since Mg^{2+} and G-actin are oppositely charged, they do not coexist at high concentrations in the same diffuse-charge layer. Mixing must thus occur during the short nonequilibrium time period as the squarewave voltage changes sign (Figure 6A). As AC frequency increases, the voltage alternates more often and should increase the amount of Mg^{2+}-G-actin formed, which is supported by the increasing slope for 10−100 Hz during the elongation regime (Figure 5C).

Enhanced mixing should occur as long as one of the species is still able to respond to the applied field. The nonequilibrium formation and dissolution of an ionic double layer can be modeled as an *RC* electrical circuit,[51] with a characteristic time scale $\tau_C = L\lambda_D/D \approx 0.1$ ms, where $L = 10$ μm is the electrode spacing, $\lambda_D = 6$ nm is the Debye screening length, and $D \approx 500$ $\mu m^2/s$ is the diffusion constant for small ions. Ionic Mg^{2+} thus has sufficient time to form a double layer in response to the applied field up to ∼10 kHz. Since this critical frequency is much faster than the frequencies where polymerization has been observed (10−200 Hz), Mg^{2+} transport is not likely to be the limiting step at higher frequencies.

Conversely, formation of stable trimeric actin nuclei is kinetically slow and is favored at low frequencies where Mg^{2+}-G-actin becomes highly concentrated and is given time to form nuclei (Figure 6B). Nucleation is nonlinear in actin concentration,[26] and will be greatly accelerated at the high concentrations within an actin double layer. At the start of the experiment most actin will be Ca^{2+} complexed, but as they mix to form Mg^{2+}−actin nucleation and growth will begin. However, the large size and low mobility of actin will limit the frequencies where actin can form a concentrated double layer. Using a typical $D \approx 50$ $\mu m^2/s$ for actin[52] the characteristic time scale for accumulating or dispersing actin at the surface is $\tau_C \approx 1.2$ ms, an order of magnitude higher than Mg^{2+}. This is consistent with the observed polymerization kinetics: no polymerization is observed at frequencies of 500 Hz or higher, where the electrode is at positive bias for 1 ms or less (equal to the half of the period of the square-wave). Even at frequencies less than 500 Hz where polymerization occurs, incomplete double layer formation increases the nucleation lag time, as found in Figure 5B. The polymerization rate in Figure 5C therefore increases up to ∼100 Hz due to enhanced mixing, then decreases at higher frequencies due to reduced nucleation and growth. Even at high frequencies where a significant fraction of actin may become Mg^{2+}-complexed, the bulk concentration of actin is too low to support nucleation without enhancement of the G-actin concentration at the electrode surface.

To summarize, we believe polymerization occurs through a three-step process: (1) G-actin is activated by Mg^{2+}-binding by mixing, (2) activated G-actin forms a stable trimeric nuclei at the electrode surface, and (3) actin filaments trapped at the electrode edges grow into large agglomerations of nematically ordered filaments. Efforts are underway to model the temporal dynamics of ion motion under a squarewave potential to understand the amount of mixing in different systems and will be addressed in future work.

Independent Control of Actin Alignment. The supramolecular organization of F-actin can be further directed through a combination of low frequency AC voltages to regulate polymer growth in conjunction with high frequency AC voltages for filament alignment through dielectrophoresis. F-actin alignment with high-frequency fields has been previously demonstrated[28] and enables trapping of filaments as well as orienting them perpendicular to the electrode surface. Since actin polymerization at low frequencies and DEP at high frequencies are independent effects, they can be applied simultaneously by superimposing the two signals. The modulation of these two mechanisms allows for independent regulation of F-actin polymerization and spatial orientation.

Dielectrophoresis occurs due to the induced dipole moment along the filament length in response to an electric field gradient.[53] For applied AC voltages with frequencies faster than $\upsilon_c = 1/\tau_C$ there is insufficient time for ion motion to screen the electric fields. Instead, these nonuniform electric fields drive the induced dipoles to orient in the direction of the field gradient. The energies of electro-orientation U_{EO} and DEP trapping U_{DEP} scale with the volume of the particle and the square of the electric field E:

$$U_{EO} = 4\pi r^2 l \varepsilon_m \varepsilon_0 \mathrm{Re}\left[\frac{(\tilde{\varepsilon}_p - \tilde{\varepsilon}_m)^2}{\tilde{\varepsilon}_m(\tilde{\varepsilon}_p + \tilde{\varepsilon}_m)}\right]E^2$$

$$U_{DEP} = \frac{\pi}{6} r^2 l \varepsilon_m \varepsilon_0 \mathrm{Re}[f_{cm}(\omega)]E^2$$

For a rod-shaped particle, r is the radius, l is the length, ε_m is the real permittivity of the medium, $\tilde{\varepsilon}_m$ and $\tilde{\varepsilon}_p$ are the complex permittivities of the medium and particle, respectively and $\mathrm{Re}[f_{cm}(\omega)] = \mathrm{Re}[(\tilde{\varepsilon}_p - \tilde{\varepsilon}_m)/\tilde{\varepsilon}_m]$ is the real part of the Clausius−Mossotti factor. For an electrode pair with a spacing of 1 μm and potential difference of 5 V, the electric field is approximately 5×10^6 V/m. Estimating $\mathrm{Re}[f_{cm}(\omega)] = 0.5$ from,[28] $r = 4$ nm and $l = 1$ μm, $U_{DEP} \approx 18\ k_B T$, indicating that the DEP trapping will overwhelm the Brownian motion of the filament.

Figure 7 shows actin filaments oriented perpendicular, rather than parallel, to the electrode surface after the application of a 1 Mhz, 10 V_{pp} (±5 V) AC voltage. Switching off the low-frequency signal while retaining the high-frequency signal

(51) Bazant, M. Z.; Thornton, K.; Ajdari, A. *Phys. Rev. E: Stat., Nonlinear, Soft Matter Phys.* **2004**, *70*, 021506.
(52) Tait, J. F.; Frieden, C. *Biochemistry* **1982**, *21*, 3666–3674.
(53) Jones, T. B., *Electromechanics of Particles*; Cambridge University Press: Cambridge, U.K., 1995.

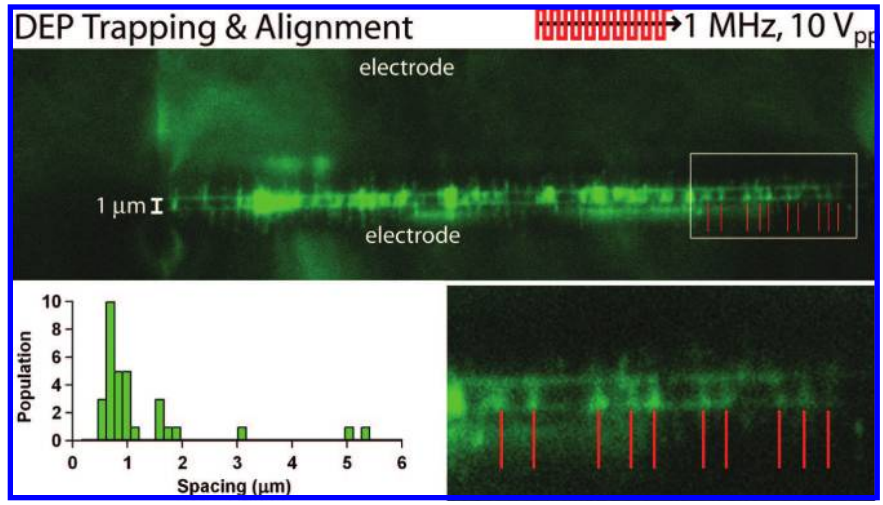

Figure 7. High-frequency AC voltages can trap and align single filaments through dielectrophoresis. This image shows a 1 MHz, 10 V_{pp} AC signal applied across a 1 μm gap. F-actin polymerization occurred for 30 s previously with an amplitude-modulated signal superimposing 1 MHz 10 V_{pp} and 100 Hz 5 V_{pp} signals.

immediately halts polymerization, but keeps the existing F-actin confined in the electrode gap. Individual actin filaments can be resolved for low filament densities. Filament density can be actively controlled by adding a low-frequency AC voltage to induce polymerization, or by decreasing the magnitude of the 1 MHz field to release shorter trapped actin filaments. It should also be noted that applying 1 MHz frequency alone never shows any actin growth or accumulation, ruling out field-induced trapping of pre-existing actin filaments within solution as the reason for the observed polymerization.

Intriguingly, in regions where filaments can be clearly distinguished they appear to have a regular spacing of approximately 700−1000 nm (Figure 7, inset). We are not able to optically resolve spacings less than 300 nm which biases the lower values; however, uniform filament spacing is observed in most samples, even with ~1 μm average spacing. It is not clear at this time how these filaments interact over such large distances, as electrostatics should be completely screened at several times the Debye screening length, or about 30 nm. This lattice-like array of actin filaments is reminiscent of artificial devices incorporating inorganic nanowires or carbon nanotubes and demonstrates the applicability of this technique for dynamically self-assembling nanostructures into ordered architectures.

Conclusions

We have demonstrated AC voltage-induced F-actin polymerization as a proof-of-concept for using electrical interfaces to dynamically regulate biomolecular self-assembly with spatial and temporal control. This phenomenon occurs through competing ionic mixing and nucleation mechanisms with opposite frequency dependences based on molecular mobilities. Since this mechanism does not require attachment of the species to the surface and can modulate activity without degrading the biological function, it is a promising route to control a range of other ion-activated protein systems with similar size and charge parameters. Moreover, the concurrent application of nonequilibrium electrokinetic forces can yield a range of complex phenomena that can be used to selectively construct highly ordered supramolecular architectures. The high filament aspect ratios and independent control of density and alignment may prove useful for the fabrication of nanoscale structures or tracks for molecular machines. Previous work has used F-actin as a precursor to template metallic nanowires,[54] and the mechanical persistence length is comparable to Si nanowires or carbon nanotubes. When combined with the extraordinary number of actin-binding proteins,[55] particularly the myosin motor protein,[56] it may be possible to dynamically assemble nanostructures with precisely controlled geometries and mechanical functionality. Given the widespread usage of divalent ions such as Ca^{2+} as an intracellular signaling messenger,[15] this scheme may be broadly applicable for regulating biomolecular structure and activity as well as the nanoscale interfaces for intracellular signaling and communication.

Experimental Details

Preparation of Proteins. G-actin (Cytoskeleton Inc., Denver CO) was stored at −80 °C and reconstituted according to instructions in G-buffer. Immediately before experiments, reconstituted G-actin samples were spun down at 100 000 rpm for 7 min in a Beckman TL100 ultracentrifuge at 4 °C to remove filaments. G-actin was diluted down to 5 μM in a low-salt (LS) buffer (0.2 mM $MgCl_2$, 2 mM KCl, 1 mM Tris, 0.2 mM ATP, 0.1 mM DTT, pH 8). 0.66 μM Alexa 488 phalloidin (Invitrogen, Carlsbad CA) to fluorescently label polymerized filaments. The critical concentration for actin in this buffer system (including phalloidin) is 9.5 +/− 0.4 μM as determined by a quantitative sedimentation assay.[29]

Electrode Fabrication. Pairs of planar microscale electrodes were fabricated on glass substrates using conventional photolithographic techniques, followed by electron-beam evaporation of 50 nm titanium. Electrode gaps in the 1−10 μm range were formed using a focused-ion beam to cut the titanium electrode. Substrates were then thoroughly cleaned for 15 min in Baker ALEG310 Photoresist Stripper (Gallade Chemical Inc., Newark, CA) and UV ozone. Device substrates and cover slides were immersed in 2 mg/mL bovine serum albumin (Sigma-Aldrich Co., St. Louis, MO) for approximately 1 h to limit nonspecific protein adsorption (Figure 1).

Characterization. The coverslips were sealed with VALAP (1:1:1 vaseline/lanolin/paraffin) to prevent evaporation at the edges that could increase the ionic salt concentration and induce poly-

(54) Patolsky, F.; Weizmann, Y.; Willner, I. *Nat. Mater.* **2004**, *3*, 692–695.
(55) Dominguez, R. *Trends. Biochem. Sci.* **2004**, *29*, 572–578.
(56) Mansson, A.; Sundberg, M.; Bunk, R.; Balaz, M.; Nicholls, I. A.; Omling, P.; Tegenfeldt, J. O.; Tagerud, S.; Montelius, L. *IEEE Trans. Adv. Packag.* **2005**, *28*, 547–555.

merization. Samples were observed on a Zeiss Axioskop 2 microscope with a 25× or 100× oil-immersion objective, epifluorescence optics and a Andor DV887 EMCCD camera. AC square-wave voltages of 10 Hz−10 kHz and 5 V_{pp} were generated using a Tektronix AFG3251 Arbitrary Function Generator. Amplitude-modulated AC signals of 5 V_{pp}, 100 Hz (carrier) and 10 V_{pp}, 1 MHz (modulation) were generated by externally triggering a Tenma 72-7650 signal generator. The use of square-wave voltages were designed to minimize electro-osmotic flow effects, which were not observed in video data. Fluorescence intensity was analyzed using Andor iQ software at 10 s intervals.

Sedimentation Assay. Sedimentation assays with G-actin (5 μM) and Alexa 488 phalloidin (0.66 μM) in LS-buffer were performed following established procedures.[29] Briefly, samples were incubated for either 4 °C overnight or for 20 min at room temperature and were spun down at 100 000 rpm for 7 min in a Beckman TL100 ultracentrifuge at 4 °C to remove filaments. Both pellets and supernatants from the centrifugation were analyzed by SDS-PAGE and it was verified that final actin concentrations were consistent with the initial sample concentration.

Bulk Polymerization Assay. Pyrene actin assays were conducted according to published methods.[50] The final assay conditions included 4.5 μM unlabeled actin and 0.5 μM pyrene-actin in buffer (10 mM Mops, 50 mM KCl, 2 mM $MgCl_2$, 2 mM EGTA, 0.2 mM ATP, 0.5 mM DTT at pH 7.0) at 24 C using an excitation wavelength of 357 nm and emission wavelength of 407 nm.

Acknowledgment. We thank V. B. Chu and S. Doniach for helpful discussions, T. Carver and E. Yenilmez for assistance with fabrication, J. Sakata for careful reading of the manuscript, and an anonymous reviewer for insightful comments on electrokinetics. I.Y.W. was supported by an NSF Graduate Research Fellowship and a Bio-X Interdisciplinary Initiatives Project.

JA7103284